

DiffStereo: High-Frequency Aware Diffusion Model for Stereo Image Restoration

Huiyun Cao*

Shenzhen International Graduate
School, Tsinghua University
Shenzhen, China
caohy22@mails.tsinghua.edu.cn

Yuan Shi*

Shenzhen International Graduate
School, Tsinghua University
Shenzhen, China
shiy22@mails.tsinghua.edu.cn

Bin Xia

Department of Computer Science and
Engineering, Chinese University of
Hong Kong
Hongkong, China
zjbinxia@gmail.com

Xiaoyu Jin

Shenzhen International Graduate
School, Tsinghua University
Shenzhen, China
jinxy22@mails.tsinghua.edu.cn

Wenming Yang[†]

Shenzhen International Graduate
School, Tsinghua University
Shenzhen, China
yang.wenming@sz.tsinghua.edu.cn

ABSTRACT

Diffusion models (DMs) have achieved promising performance in image restoration but haven't been explored for stereo images. The application of DM in stereo image restoration is confronted with a series of challenges. The need to reconstruct two images exacerbates DM's computational cost. Additionally, existing latent DMs usually focus on semantic information and remove high-frequency details as redundancy during latent compression, which is precisely what matters for image restoration. To address the above problems, we propose a high-frequency aware diffusion model, DiffStereo for stereo image restoration as the first attempt at DM in this domain. Specifically, DiffStereo first learns latent high-frequency representations (LHFR) of HQ images. DM is then trained in the learned space to estimate LHFR for stereo images, which are fused into a transformer-based stereo image restoration network providing beneficial high-frequency information of corresponding HQ images. The resolution of LHFR is kept the same as input images, which preserves the inherent texture from distortion. And the compression in channels alleviates the computational burden of DM. Furthermore, we devise a position encoding scheme when integrating the LHFR into the restoration network, enabling distinctive guidance in different depths of the restoration network. Comprehensive experiments verify that by combining generative DM and transformer, DiffStereo achieves both higher reconstruction accuracy and better perceptual quality on stereo super-resolution, deblurring, and low-light enhancement compared with state-of-the-art methods.

CCS CONCEPTS

• **Computing methodologies** → **Reconstruction; Matching;**

KEYWORDS

Stereo Image Restoration, Diffusion Model, Transformer

1 INTRODUCTION

Stereoscopic imaging systems shoot a scene from left and right perspectives. According to the geometric relationship in a stereo

pair, the parallax between the two views and the depth of objects can be calculated and further we can analyze the 3D structure of the scene. Stereo cameras and stereo images have been extensively used in diverse 3D applications, such as mobile robot navigation, automatic driving [19], virtual reality [12], and augmented reality [28]. Stereo image restoration aims to reconstruct high-quality (HQ) stereo images from their low-quality (LQ) counterparts corrupted by various degradation factors. The reconstruction of HQ stereo images can significantly benefit downstream tasks, such as depth estimation, 3D object detection, 3D scene rendering and reconstruction, and image segmentation. Therefore, stereo image restoration has important theoretical significance and practical value.

Existing stereo image restoration methods are based on convolutional neural network (CNN) or transformer, which have achieved pronounced effectiveness. However, the two kinds of methods have some drawbacks, respectively. CNN-based methods [2, 4, 18, 39, 44, 45, 47, 49, 50, 52] suffer from limited local receptive fields and seem difficult to improve the reconstruction performance of stereo images further. Transformer-based methods [10, 24, 51] are constrained by the computational burden of intrinsic self-attention layer and restoring both view images. Most transformer-based methods perform cross-view interaction in the same way as PAM in essence or within a local window like SwinIR [22], limiting transformer's ability to model long-range context dependencies.

In recent years, diffusion models (DMs) [13, 37] have aroused great concern due to their superior performance of generating a wide variety of data modalities, including vision [5, 6, 13, 38, 40], natural language [41] and audio [17]. A diffusion probabilistic model is a parameterized Markov chain trained with variational inference to produce samples matching the data after finite time. In the forward process, Gaussian noise is gradually added to the input image until it becomes pure noise. When the intensity of the Gaussian noise sequence is low enough, the reverse transitions of this chain can be set to conditional Gaussian too. Then the reverse distribution can be parameterized by a simple neural network. Samples can be generated based on the estimated reverse distribution.

Motivated by the fact that DMs can model highly complex distributions of natural images, we aim to take advantage of the powerful

*Both authors contributed equally to this research.

[†]Corresponding author.

distribution estimation abilities of DMs to assist the texture recovery in degraded images. However, the utilization of DMs for stereo image restoration is confronted with the following challenges: Firstly, the training and inference of diffusion models are computationally expensive. In stereo image restoration, images of left and right views need to be reconstructed simultaneously, which exacerbates the effect of high computational cost of DM. The majority of DM-based image restoration algorithms [5, 21, 27, 31, 33] perform the diffusion process in the image space, which requires thousands of iterations to generate each pixel from noise. It is infeasible to directly apply the paradigm of existing DM-based image restoration algorithms to stereo images. Secondly, existing restoration methods utilize DM to generate the HQ image or its latent embedding, which is then converted to the pixel space. In this manner, DM directly affects the recovery results and is prone to generate some details which are perceptually high-quality but misaligned with the given LQ image. It can be observed a drop of accuracy related metrics (e.g., PSNR) in these methods compared to CNN and transformer. Thirdly, previous latent compression methods [7, 20, 30, 42] are primarily devised for image synthesis, in which the latent representation focuses on high-level semantics. High-frequency details are removed as redundancy, which are exactly pivotal for low-level restoration. For stereo image restoration, how to preserve the high-frequency details and achieve efficient compression in the meantime is a crucial problem.

To address the above issues, we propose DiffStereo, the first diffusion model-based framework for stereo image restoration. Due to the high computational overhead in the image space, we perform the diffusion process in a compressed latent space, whose dimensions are lower than that of the image space. Contrary to previous latent compression methods, DiffStereo is trained to estimate a latent representation preserving high-frequency details of HQ images. The resolution of latent high-frequency representations (LHFR) is kept the same as input images with channel compressed, preventing the inherent texture of input from distortion. The LHFR are then fused into transformer-based restoration network to guide the texture recovery in degraded images, supplementing high-frequency information of corresponding HQ images. The combination of DM and transformer also overcomes the influence of artifacts introduced by DM, ensuring the fidelity of the restored images.

In summary, our main contributions are as follows:

- We propose a high-frequency aware diffusion model DiffStereo, which is the first DM for stereo image restoration. DiffStereo combines the powerful distribution estimation ability of DM and long-range modeling superiority of transformer and achieves better perceptual quality and higher accuracy.
- DiffStereo leverages DM to generate high-frequency representations of HQ images in a compressed latent space, which are fused into transformer-based restoration network. Meanwhile, we design a position encoding scheme to integrate the latent representations into the restoration network.
- Extensive experiments conducted on super-resolution (SR), deblurring, and low-light enhancement demonstrate the superior performance of DiffStereo compared with state-of-the-art stereo image restoration methods.

2 RELATED WORK

2.1 Stereo Image Restoration

The dominant stereo image restoration models are based on CNN or transformers. StereoSR [18] is the first deep learning-based algorithm for stereo image SR, which shifts the right view by 1 to 64 pixels and cascades the shifted images with the left view. Then StereoSR fuses the cross-view information by applying convolution to the cascaded images. In this way, for a pixel with parallax less than 64, there must be its corresponding point in one of the shifted images. But pixels with parallax larger than 64 cannot utilize their complementary information, which limits reconstruction performance. PASSR [45] integrates epipolar constraints in binocular vision with self-attention mechanism and proposes a parallax attention mechanism (PAM). PAM calculates the similarity between pixels on the same epipolar line and fuses complementary features based on the calculated similarity, which becomes a crucial method for stereo parallax interaction and widely adopted by [2, 39, 44, 47, 49, 52]. The other kind of algorithms [4, 50] predict pixel-level disparity explicitly and align features of two views according to the disparity map. Recently, transformer has been introduced into stereo image restoration [10, 24, 51]. However, there hasn't been any research focusing on diffusion model for stereo image restoration. In this paper, we make the first attempt in this field.

2.2 Diffusion Models

In recent years, diffusion models have achieved outstanding results in deep generative modeling across various modal domains, such as image [5, 13, 32, 38, 40], video [6, 36], natural language [41], audio [17] and 3D [25]. In image restoration, [21] propose the first DM-based single image SR algorithm SRDiff. SR3 [33] adapts DMs to conditional image generation and performs SR through an iterative denoising process. Afterwards, a variety of DM-based image restoration studies have been proposed [5, 8, 27, 31?]. However, the algorithms listed above perform the diffusion process on whole images, which requires thousands of iteration steps to generate each pixel from noise. LDM [30] proposes to perform DM in latent space to improve the restoration efficiency. Furthermore, DiffIR [48] proposes to adopt DM to generate a compact vector for image restoration.

3 METHOD

3.1 Overview

Existing DM-based image restoration algorithms follow the paradigm of DM in image synthesis, which generates the whole image or its latent embedding directly. Generating the whole image using a DM typically requires thousands of iterations. In image restoration, it is a waste of computing resources since a part of pixels are already given in the LQ image. Alternatively, if we apply the diffusion process to the embedding of an image, elaborate encoder and decoder are required to convert images between the image space and latent space. Furthermore, the latent compression in image synthesis focuses on high-level semantics with low-level high-frequency details discarded by commonly used downsampling, which isn't suitable for image restoration.

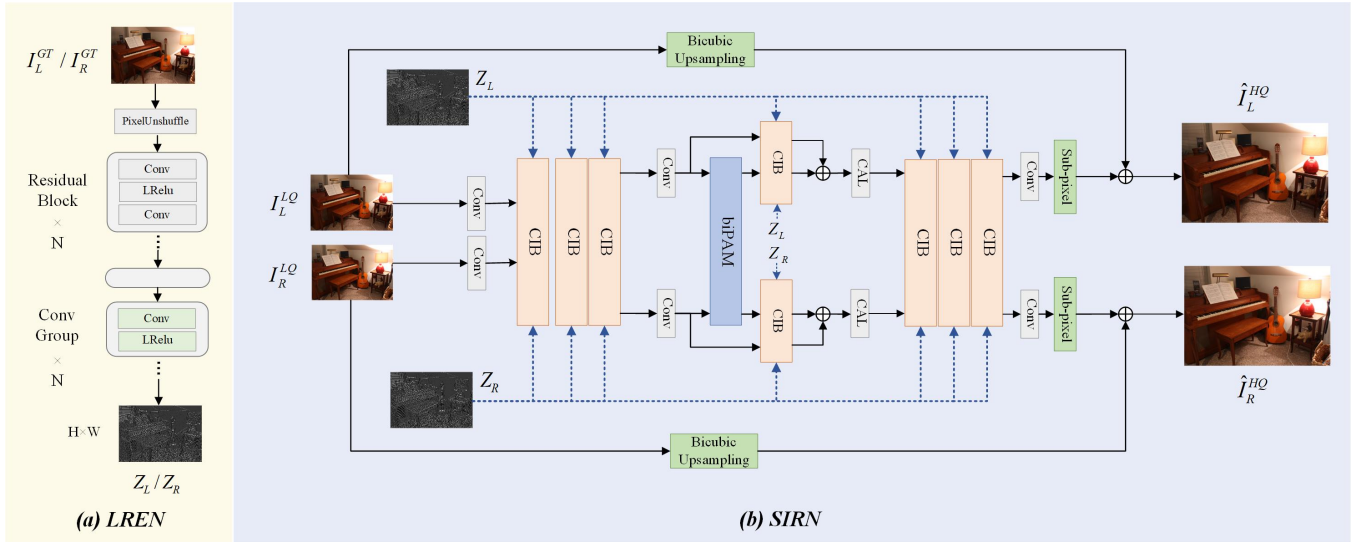


Figure 1: An overview of DiffStereo in training stage one. The latent representation extraction network (LREN) learns a compressed latent space which preserves high-frequency details like structural information and texture in HR stereo images and obtains LHFR of left and right views. The LHFR are then fused into stereo image restoration network (SIRD) and assist the texture recovery.

The key of DiffStereo is to apply the diffusion model in latent space and estimate latent high-frequency representations (LHFR) of HQ images, which acts as a guidance for the transformer-based restoration network. In this way, DiffStereo combines the strengths of DM and transformer. The DM learns the complex target distribution of stereo images, providing beneficial prior about real distribution. And the regression-based transformer achieves high precision image recovery.

Our DiffStereo is composed of three parts: latent representation extraction network (LREN), high-frequency aware DM and stereo image restoration network (SIRD). During training, the LREN first learns high-frequency representations from the HQ stereo images. The diffusion model then learns to estimate the LHFR given LQ images, approximating the output of the LREN. To make the overall framework easier to optimize, we train DiffStereo with a two-stage training strategy, which we will explain in detail in this section.

3.2 Training Stage One

In the first stage, we train the latent representation extraction network (LREN) and stereo image restoration network (SIRD) together to enforce the LREN to learn high-frequency representations conducive to restoration.

3.2.1 Latent Representation Extraction Network (LREN). To extract the LHFR from HQ images, we first downsample the HQ stereo images by PixelUnshuffle operation and extract deep features by stacked residual blocks. Next, several groups of convolution and LeakyReLU are set to compress the channels of the feature maps. The structure of LREN is shown in Fig. 1(a). The outputs are 2D latent high-frequency representations $Z_L, Z_R \in \mathbb{R}^{H \times W}$, acting as guidance for stereo image restoration.

3.2.2 Stereo Image Restoration Network (SIRD). For stereo image restoration, we design a transformer-based network considering the fact that transformer can model long-range pixel dependencies. Restormer [53] introduces a multi-Dconv head transposed attention with linear complexity which applies self-attention across feature dimension rather than the spatial dimension. Inspired by the idea, we devise a channel interaction block (CIB) as the basic unit of our SIRD. CIB concatenates the features of the two views and uses all pixels from the two views to calculate a channel attention map shared by the two views. In the process of stereo imaging, since the left and right images are shot, transmitted and stored at the same time, they suffer from the same degradation and have the same distribution. Thus the channel covariance should be the same too. Taking account of all pixels in the two views is beneficial to obtaining more accurate channel covariance.

In each CIB, layer normalization is first applied to the input features X_L and $X_R \in \mathbb{R}^{C \times H \times W}$. 1×1 convolutions encode pixel-wise channel context, followed by 3×3 depth-wise convolutions aggregating channel-wise spatial context. We reshape output of the convolutions to $\mathbb{R}^{head \times \hat{C} \times HW}$ and obtain query (Q), key (K), and value (V) of the two views. Then we concatenate Q_L and Q_R , K_L and K_R along the spatial dimension,

$$\begin{aligned} Q &= \text{Concat}(Q_L, Q_R) \\ &= \text{Concat}(W_d^Q W_p^Q \text{LN}(X_L), W_d^Q W_p^Q \text{LN}(X_R)) \end{aligned} \quad (1)$$

$$\begin{aligned} K &= \text{Concat}(K_L, K_R) \\ &= \text{Concat}(W_d^K W_p^K \text{LN}(X_L), W_d^K W_p^K \text{LN}(X_R)) \end{aligned} \quad (2)$$

$$V_{L/R} = W_d^V W_p^V \text{LN}(X_{L/R}) \quad (3)$$

where $W_p^{(\cdot)}$ is 1×1 point-wise convolution and $W_d^{(\cdot)}$ is 3×3 depth-wise convolution. Then multi-Dconv head transposed attention is

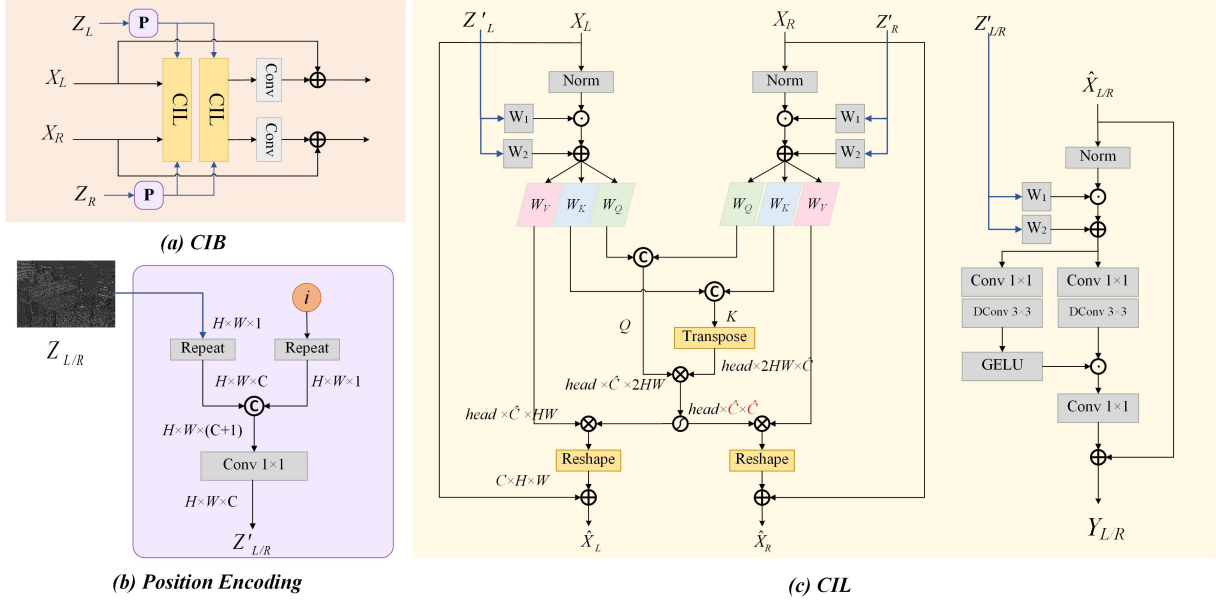


Figure 2: The architecture of our proposed: (a) channel interaction block (CIB), (b) Position Encoding scheme, (c) channel interaction layer (CIL) in CIB.

calculated and generates channel attention map $A \in \mathbb{R}^{head \times \hat{C} \times \hat{C}}$ shared by the two views and enhanced stereo features \hat{Y}_L and $\hat{Y}_R \in \mathbb{R}^{C \times H \times W}$,

$$\hat{Y}_{L/R} = \text{Attention}(Q, K, V_{L/R}) = \text{Softmax}(Q \cdot K^T / w) \cdot V_{L/R} \quad (4)$$

where w is a learnable scaling factor. \hat{Y}_L and \hat{Y}_R are then sent into gated-Dconv feed-forward network (GDFN) [53] and generate the final output of CIB Y_L and $Y_R \in \mathbb{R}^{C \times H \times W}$, which is defined as,

$$Y_{L/R} = \text{GDFN}(\hat{Y}_{L/R} + X_{L/R}) \quad (5)$$

3.2.3 Position Encoding Scheme. We propose a position encoding scheme when integrating the LHFR into restoration network in order to provide distinctive priors for CIBs of different depths. The position index i is generated based on the depth of each CIB in SIRN. The CIB of the first layer corresponds to index 0 and the index increases in ascending order in following layers. We copy the index into a matrix $I \in \mathbb{R}^{H \times W \times 1}$. Before integrating the LHFR into each CIB, we extend the dimension of Z_L, Z_R to $\mathbb{R}^{H \times W \times 1}$ and copy them C times along the channel and concatenate the repeated LHFR with I . The two features are fused by 1×1 point-wise convolution and generate encoded $Z'_L, Z'_R \in \mathbb{R}^{H \times W \times C}$, the same shape as X_L and X_R . Then $Z'_L, Z'_R \in \mathbb{R}^{H \times W \times C}$ are fused with the features in CIB in a way of spatial modulation,

$$X'_{L/R} = W_1 Z'_{L/R} \odot \text{LN}(X_{L/R}) + W_2 Z'_{L/R} \quad (6)$$

where W_1 and W_2 denote weights of convolution layers.

3.3 Training Stage Two

In the second stage, the high-frequency aware DM and stereo image restoration network (SIRN) are optimized together to enforce DM

to estimate the high-frequency latent representations given LQ images, approximating the output of the LREN.

Using the pretrained LREN in Stage One, the groundtruth LHFR are extracted and denoted as $Z_L, Z_R \in \mathbb{R}^{H \times W}$. We apply the forward diffusion process on Z_L, Z_R and the noised LHFR are sampled by,

$$q(Z_{L,T} | Z_L) = \mathcal{N}(Z_{L,T}; \sqrt{\alpha_T} Z_L, (1 - \alpha_T) \mathbf{I}) \quad (7)$$

$$q(Z_{R,T} | Z_R) = \mathcal{N}(Z_{R,T}; \sqrt{\alpha_T} Z_R, (1 - \alpha_T) \mathbf{I}) \quad (8)$$

where T is the total number of iterations, $Z_{L,T}$ and $Z_{R,T}$ are the LHFR of left and right view at time step T . $\bar{\alpha}_T = \prod_{i=0}^T \alpha_i$, α_i is the variance schedule.

In the reverse process, the diffusion model learns the reverse transitions of the Markov chain, which is a conditional Gaussian distribution denoted as,

$$q(Z_{t-1} | Z_t, Z_0) = \mathcal{N}(Z_{t-1}; \mu_t(Z_t, Z_0), \sigma_t^2 \mathbf{I}), \quad (9)$$

$$\mu_t(Z_t, Z_0) = \frac{1}{\sqrt{\alpha_t}} \left(Z_t - \frac{1 - \alpha_t}{\sqrt{1 - \alpha_t}} \epsilon_t \right), \sigma_t^2 = \frac{1 - \bar{\alpha}_{t-1}}{1 - \bar{\alpha}_t} \beta_t. \quad (10)$$

where ϵ_t represents the noise added in Z_t , which is the only unknown term in the posterior distribution. The subscripts L and R denoting left and right view are omitted for simplicity. We can use a particularly simple neural network θ to estimate $\hat{\epsilon}_t$ and Z_{t-1} can be sampled by parameterizing the Gaussian distribution,

$$\hat{Z}_{t-1} = \frac{1}{\sqrt{\alpha_t}} \left(\hat{Z}_t - \frac{1 - \alpha_t}{\sqrt{1 - \alpha_t}} \hat{\epsilon}_t \right) \quad (11)$$

The process in Eq. (11) is iterated T times until the pure LHFR \hat{Z}_L, \hat{Z}_R are recovered. It is worth noting that the random term following

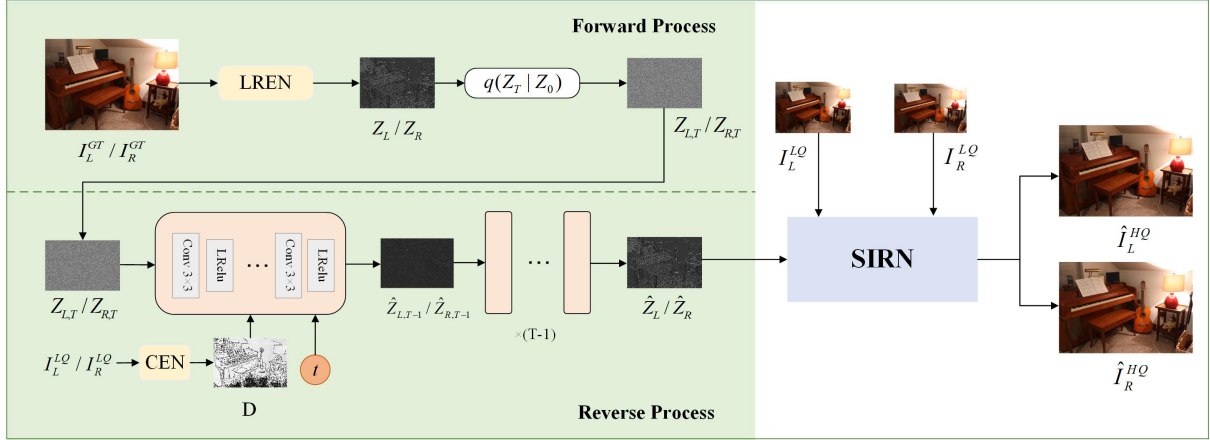


Figure 3: An overview of DiffStereo in training stage two. The DM learns to estimate the LHFR extracted by pretrained LREN, whose parameters are frozen in stage two. During inference, the DM estimates LHFR from pure Gaussian noise under the guidance of LR stereo images.

standard normal distribution with a coefficient of σ_t is deleted for better image fidelity.

The denoising network θ is expected to predict a sequence of noise to recover a LHFR corresponding to the given LQ image. Thus we first adopt a simple CNN network, denoted as CEN (condition extraction network) to obtain a conditional feature $D \in \mathbb{R}^{H \times W}$ from given LQ image. D is then sent into the denoising network θ for noise prediction with the encoded spatial information of LQ image as well as the timestep t , which is described as,

$$\hat{\epsilon}_t = \theta(\text{Concat}(\hat{Z}_t, D, t)) \quad (12)$$

3.4 Loss Functions

Reconstruction Loss. The reconstruction loss is the L_1 distance between the restored and groundtruth stereo images:

$$\mathcal{L}_{rec} = \left\| \hat{I}_L^{HQ} - I_L^{GT} \right\|_1 + \left\| \hat{I}_R^{HQ} - I_R^{GT} \right\|_1 \quad (13)$$

where \hat{I}_L^{HQ} and \hat{I}_R^{HQ} are restored high-quality left and right images, I_L^{GT} and I_R^{GT} are the groundtruth left and right images.

Parallax Related Loss. Following [47], we use smoothness loss, residual photometric loss, residual cycle loss and residual stereo consistency loss to supervise the network to estimate disparity correlations between left and right view accurately. We denote these terms as parallax related loss \mathcal{L}_{para} .

Diffusion Related Loss. The optimization of denoising diffusion probabilistic models in [13] is implemented by,

$$\nabla_{\theta} \left\| \epsilon - \epsilon_{\theta}(\sqrt{\alpha_t}x_0 + \sqrt{1 - \alpha_t}\epsilon, t) \right\|^2 \quad (14)$$

where t is uniformly sampled from $\{1, \dots, T\}$. Since in DiffStereo, the DM only needs to estimate LHFR whose dimensions are much lower than that of the original image, it's feasible to run all iterations of DM at a time and train the DM by the distance between estimated \hat{Z}_L, \hat{Z}_R by DM and Z_L, Z_R extracted by LREN,

$$\mathcal{L}_{diff} = \|\hat{Z}_L - Z_L\|_1 + \|\hat{Z}_R - Z_R\|_1 \quad (15)$$

In the first stage, reconstruction loss and parallax related loss are utilized to train the LREN and SIRD, which is defined as follows:

$$\mathcal{L}_{stage1} = \mathcal{L}_{rec} + \lambda_1 * \mathcal{L}_{para} \quad (16)$$

where λ_1 represents the weight of parallax related loss is set to 0.1 in this work. In the second stage, diffusion related loss is also included in the overall training objective,

$$\mathcal{L}_{stage2} = \mathcal{L}_{rec} + \lambda_1 * \mathcal{L}_{para} + \lambda_2 * \mathcal{L}_{diff} \quad (17)$$

where λ_2 represent the weight of diffusion model related loss, set to 0.25 in this work.

4 EXPERIMENTS

4.1 Datasets and Implementation Details

Datasets. For SR, we construct our training and test set following the previous works [18, 45, 47, 52]. 800 images from the training set of Flickr1024 [46] and 60 images from Middlebury [34] make up the training data. For test set, we use 5 images from Middlebury [34], 20 images from KITTI 2012 [9], 20 images from KITTI 2015 [26] and all the 112 images from the test set of Flickr1024 [46]. Low-resolution images are generated by bicubic downsampling the HQ images. For deblurring, we use the same HQ images as in SR. And we convolve the HQ images with a Gaussian blur kernel whose kernel size is 15×15 and σ is 1.0 to generate LQ images. For low-light enhancement, we use the synthetic Holopix50k [16] dataset, which is generated by adopting linear transformation and gamma correction for the normal-light images [15] to reduce lightness and then adding Gaussian-Poisson mixed noise. For all of the three tasks, we crop LQ images into 30×90 patches with a stride of 20 before training. Randomly flipping horizontally and vertically is applied for data augmentation.

Implementation Details. DiffStereo is implemented in PyTorch and trained with two NVIDIA RTX 3090 GPU. We use the Adam optimizer with $\beta_1 = 0.9$ and $\beta_2 = 0.999$ and the batch size is set to 48. DiffStereo is trained for 90 epochs in the first stage and 300 epochs in the second stage.

Table 1: Quantitative comparisons for $\times 4$ SR with PSNR/SSIM/FID values. Higher PSNR/SSIM and lower FID mean better performance. Red and blue colors represent the best and second best performance, respectively.

Method	PSNR \uparrow / SSIM \uparrow / FID \downarrow / LPIPS \downarrow			
	Flickr1024	KITTI2012	KITTI2015	Middlebury
EDSR	23.46/0.7285/0.1797/0.2672	26.35/0.8015/0.2655/0.1965	26.04/0.8039/0.1959/0.1565	29.23/0.8397/0.1985/0.1584
RDN	23.47/0.7295/0.1529/ 0.2648	26.32/0.8014/ 0.2621/0.1949	26.04/0.8043/0.1990/ 0.1547	29.27/0.8404/0.1926/ 0.1577
RCAN	23.48/0.7286/0.1828/0.2705	26.44/0.8029/0.2773/0.2042	26.22/0.8068/0.2034/0.1590	29.30/0.8397/0.1994/0.1603
StereoSR	21.70/0.6460/0.1856/0.2937	24.53/0.7556/0.3049/0.2072	24.21/0.7511/0.2554/0.1931	27.64/0.8022/0.2496/0.1709
PASSRnet	23.31/0.7195/0.1638/0.2871	26.34/0.7981/0.2622/0.2095	26.08/0.8002/ 0.1880 /0.1606	28.72/0.8236/0.2305/0.1969
SRRes+SAM	23.27/0.7233/ 0.1450 /0.2772	26.44/0.8018/0.2665/0.2122	26.22/0.8054/0.1962/0.1667	28.83/0.8290/ 0.1966 /0.1721
iPASSR	23.44/0.7287/0.1815/0.2713	26.56/0.8053/0.2674/0.2076	26.32/0.8084/0.1971/0.1614	29.16/0.8367/0.2048/0.1657
SSRDE-FNet	23.55/0.7346 /0.1765/0.2695	26.69/0.8091 /0.2749/0.2074	26.46/0.8133 /0.2000/0.1566	29.34/0.8411 /0.2039/0.1713
SIR-Former	23.52/0.7305/ - / -	26.68 /0.8077/ - / -	26.42/0.8098/ - / -	29.32/0.8407/ - / -
DiffStereo (Ours)	23.60/0.7379/0.1460/0.2603	26.67/0.8081/0.2612/0.1944	26.46/0.8148/0.1961/0.1516	29.41/0.8441/0.1913/0.1559



Figure 4: Visual comparisons for $\times 4$ SR by different methods on Flickr1024 and Middlebury dataset.

Table 2: Quantitative comparisons for deblurring with PSNR/SSIM values. Higher PSNR and SSIM mean better performance. Red color represents the best performance, respectively.

Method	Params	Left			(Left + Right) / 2			
		KITTI2012	KITTI2015	Middlebury	Flickr1024	KITTI2012	KITTI2015	Middlebury
PASSRnet	1.37M	37.87/0.9675	36.94/0.9699	40.33/0.9768	37.10/0.9751	37.88/0.9682	37.53/0.9726	40.34/0.9768
iPASSR	1.43M	38.63/0.9719	38.07/0.9766	41.13/0.9802	38.09/ 0.9793	38.60/0.9723	38.71/0.9788	41.17/0.9802
DiffStereo (Ours)	2.16M	38.78/0.9721	38.33/0.9771	41.34/0.9804	38.13/0.9790	38.74/0.9724	38.98/0.9793	41.37/0.9804

Evaluation Metric. Following previous works, we adopt peak signal-to-noise ratio (PSNR) and structural similarity index metrics (SSIM) to measure the accuracy of reconstructed images. Furthermore, we use Frechet inception distance score (FID) to measure the

distance between the real image distribution and the restored image distribution. Learned perceptual image patch similarity (LPIPS) is also adopted to evaluate the perceptual quality of reconstructed images.



Figure 5: Visual comparisons in Low-Light Enhancement by different methods.

Table 3: Comparisons of different low-light enhancement methods in terms of PSNR, SSIM, FID and LPIPS.

Method	PASSRnet	iPASSR	DiffStereo (Ours)
PSNR \uparrow	25.43	26.69	27.48
SSIM \uparrow	0.8864	0.9048	0.9076
FID \downarrow	0.0910	0.0586	0.0454
LPIPS \downarrow	0.0557	0.0446	0.0459

4.2 Comparisons with State-of-the-Art Methods

In this section, we compare the proposed DiffStereo with SOTA restoration methods on SR, deblurring and low-light enhancement. For fair comparisons, all the methods below are trained with the same datasets and data augmentation strategies.

4.2.1 Stereo Image Super-Resolution. As displayed in Table 1, we compare the proposed DiffStereo with single image SR methods EDSR [23], RDN [55], RCAN [54] and stereo image SR methods StereoSR [18], PASSRnet [45], SRRes+SAM [52], iPASSR [47], SSRDE-FNet [4] and SIR-Former [51]. FID and LPIPS of SIR-Former aren’t given because its source code isn’t publicly available. In terms of reconstruction accuracy, DiffStereo achieves comparable PSNR/SSIM on KITTI2012 and KITTI2015 datasets and better PSNR/SSIM on Flickr1024 and Middlebury datasets. At the aspect of FID, DiffStereo surpasses SOTA method SSRDE-FNet by 0.0305, 0.0137, 0.0039, 0.0126, which means the stereo image distribution estimated by DiffStereo is closer to the real distribution than that of SSRDE-FNet. This is owing to the powerful distribution estimation ability of diffusion model. For LPIPS, DiffStereo outperforms other methods on all the four datasets, fully proving that the introduction of DM can benefit the perceptual quality of restored images. In general, our DiffStereo achieves the best balance between reconstruction accuracy, distribution estimation and perceptual quality by the effective combination of transformer and DM. Qualitative comparisons are shown in Fig. 4. It’s obvious that our DiffStereo can recover richer details and clearer edges compared with other SOTA methods.

4.2.2 Stereo Image Deblurring. To evaluate the generalization ability of DiffStereo, we also compare it on stereo deblurring task with representative methods PASSRnet [45] and iPASSR [47]. It can be

observed from Table 2 that DiffStereo surpasses iPASSR by up to 0.27 dB, demonstrating the superiority of DiffStereo in deblurring.

4.2.3 Stereo Image Low-Light Enhancement. On stereo low-light enhancement task, DiffStereo achieves a significant improvement of 0.79 dB in terms of PSNR compared with iPASSR. The obvious gain of PSNR, SSIM and FID substantiates the generalization of our DiffStereo. And DiffStereo is able to adapt to changes in light conditions in a wide variety of realistic scenarios of Holopix50k.

4.3 Ablation Study

4.3.1 Effectiveness of Latent High-Frequency Representations (LHFR).

We conduct the following three experiments to illustrate the importance of high-frequency aware compression and the effectiveness of LHFR: (1) The LHFR estimated by diffusion model are not introduced into SIRN. (2) The LHFR are replaced with 1D channel vectors $Z \in \mathbb{R}^C$. (3) The original LHFR $Z \in \mathbb{R}^{H \times W}$ used in DiffStereo. Comparing (1) with (2) and (3), it is obvious that the latent representations estimated by DM benefit the quality of reconstruction in terms of PSNR and SSIM. Particularly, the LHFR improve the restoration performance significantly. Furthermore, in our settings, $C = 256$, $H = 30$ and $W = 90$, so the compression ratios of the two kinds of latent representations are almost the same during training. But the LHFR work much better than 1D vectors, which means the spatial structure information is more rewarding than global semantics for restoration. As shown in Fig. 6, we visualize the LHFR Z_L, Z_R extracted from HQ images in the first stage and \hat{Z}_L, \hat{Z}_R estimated by DM at various timesteps. Under the constraint of reconstruction loss, the latent representations learned by DiffStereo indeed focus on high-frequency edges. And given LR images, DM is capable of perceiving high-frequency information in HQ images, taking only a few denoising iterations.

Furthermore, we assess the role of LHFR generated by DM on SR, deblurring and low-light enhancement. The quantitative results are shown in Table 5. On all datasets for all tasks, there is a consistent and significant improvement of PSNR. Especially, the LHFR bring a gain of 0.57 dB on Middlebury dataset for deblurring.

4.3.2 Effectiveness of the Position Encoding. To explore the effectiveness of position encoding proposed in DiffStereo, we evaluate PSNR and SSIM with and without the position encoding scheme. As displayed in Table 4, the position encoding scheme can further

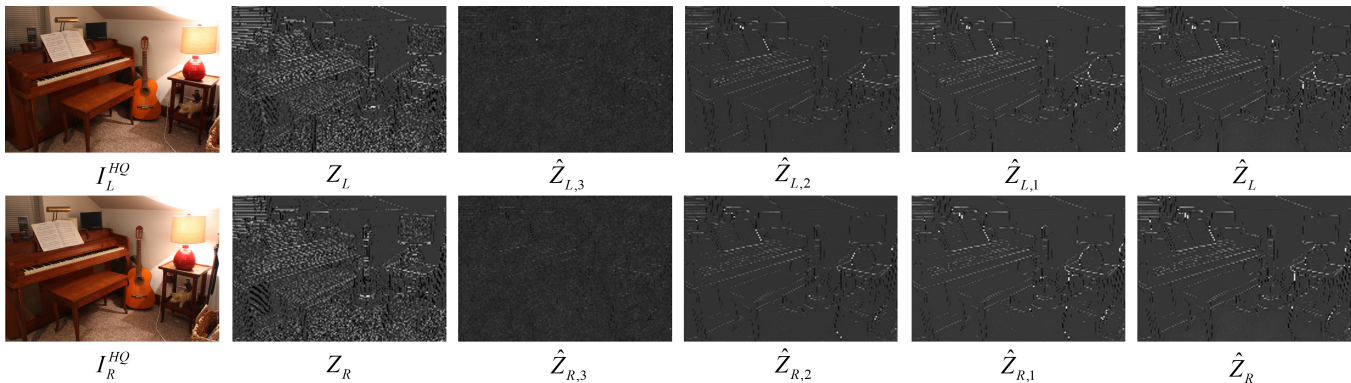


Figure 6: Visualizations of LHFR in different training stages and different timesteps of denoising. The total timestep T is set to 4 since more iterations do not provide further improvement.

Table 4: Quantitative comparisons for different latent representations and Position Encoding (*i.e.*, PE) in terms of PSNR/SSIM.

	1D vector	LHFR	PE	Stage	Flickr1024	KITTI2012	KITTI2015	Middlebury
1	×	×	×	-	23.53/0.7347	26.64/0.8079	26.39/0.8117	29.34/0.8409
2	✓	×	×	1	23.59/0.7366	26.70/0.8083	26.51/0.8135	29.33/0.8411
3	×	✓	×	1	26.98/0.8704	29.43/0.8883	28.71/0.8860	32.85/0.9227
4	×	✓	✓	1	27.15/0.8748	29.53/0.8902	28.78/0.8878	33.07/0.9259

Table 5: Comparisons of DiffStereo with and without (*i.e.*, w/o) LHFR (*i.e.*, LR) on SR, deblurring and low-light enhancement (*i.e.*, LLE).

Task	Dataset	PSNR		SSIM	
		w/o LR	with LR	w/o LR	with LR
SR	Flickr1024	23.53	23.60	0.7342	0.7379
	KITTI2012	26.65	26.67	0.8079	0.8081
	KITTI2015	26.41	26.46	0.8118	0.8148
	Middlebury	29.30	29.41	0.8399	0.8441
Deblur	Flickr1024	37.79	38.13	0.9790	0.9790
	KITTI2012	38.43	38.74	0.9725	0.9724
	KITTI2015	38.42	38.98	0.9790	0.9793
	Middlebury	40.80	41.37	0.9803	0.9804
LLE	Holopix50k	27.42	27.48	0.9067	0.9076

Table 6: Comparisons of different structures of SIRN.

	Flickr1024	KITTI2012	KITTI2015	Middlebury
NAFB	23.24	26.36	26.05	29.05
RDB	23.43	26.56	26.30	29.18
CIB	23.59	26.64	26.41	29.39

improve the restoration performance on the basis of LHFR comparing (3) and (4). It is suggested that providing distinctive priors in different depths of image restoration network can help the network to recover image details better.

4.3.3 *Effectiveness of CIB in Stereo Image Restoration Network.* In order to study which type of restoration network matches DM better, we replace the proposed CIB with commonly used residual dense block (RDB) and nonlinear activation free block (NAFB) [3] in image restoration. It can be observed from Table 6 that CIB outperforms both RDB and NAFB by a significant margin, highlighting the effectiveness of our proposed CIB. The results demonstrate that the latent representations generated by DM is more suitable to a transformer-based structure. The combination of the CIB block and DM can achieve superior performance in image restoration tasks.

5 CONCLUSION

In this paper, we propose a novel high-frequency aware diffusion model for stereo image restoration as the first attempt of DM in this domain. Contrary to previous latent compression methods focusing on high-level semantics, DiffStereo is trained to preserve high-frequency details of HQ images and utilizes the DM to generate latent high-frequency representations compressed from groundtruth HQ images, which are sent into a transformer-based stereo image restoration network serving as guidance. The implementation of diffusion process in a compact latent space significantly alleviates the massive computational burden typically associated with diffusion models. Importantly, the LHFR synthesized by the DM does not directly intervene in the image restoration process, thereby minimizing the effect of artifacts introduced by DM. Meanwhile the high-frequency details of HQ images and real distribution information encoded in the LHFR substantially boost the stereo image restoration performance, exerting the distribution estimation ability of DM. Extensive experiments on super-resolution, deblurring and low-light enhancement demonstrate that DiffStereo achieves

superior results in both accuracy and perceptual quality compared with SOTA methods.

REFERENCES

- [1] Andreas Blattmann, Robin Rombach, Huan Ling, Tim Dockhorn, Seung Wook Kim, Sanja Fidler, and Karsten Kreis. 2023. Align your latents: High-resolution video synthesis with latent diffusion models. In *CVPR*.
- [2] Canqiang Chen, Chunmei Qing, Xiangmin Xu, and Patrick Dickinson. 2021. Cross parallax attention network for stereo image super-resolution. *IEEE TMM* (2021).
- [3] Liangyu Chen, Xiaojie Chu, Xiangyu Zhang, and Jian Sun. 2022. Simple baselines for image restoration. In *ECCV*.
- [4] Qinyan Dai, Juncheng Li, Qiaosi Yi, Faming Fang, and Guixu Zhang. 2021. Feed-back network for mutually boosted stereo image super-resolution and disparity estimation. In *ACM MM*.
- [5] Prafulla Dhariwal and Alexander Nichol. 2021. Diffusion models beat gans on image synthesis. *NeurIPS* (2021).
- [6] Patrick Esser, Johnathan Chiu, Parmida Atighehchian, Jonathan Granskog, and Anastasis Germanidis. 2023. Structure and content-guided video synthesis with diffusion models. In *CVPR*.
- [7] Patrick Esser, Robin Rombach, and Bjorn Ommer. 2021. Taming transformers for high-resolution image synthesis. In *CVPR*.
- [8] Sicheng Gao, Kuhui Liu, Bohan Zeng, Sheng Xu, Yanjing Li, Xiaoyan Luo, Jianzhuang Liu, Xiantong Zhen, and Baochang Zhang. 2023. Implicit diffusion models for continuous super-resolution. In *CVPR*.
- [9] Andreas Geiger, Philip Lenz, and Raquel Urtasun. 2012. Are we ready for autonomous driving? the kitti vision benchmark suite. In *CVPR*.
- [10] Hansheng Guo, Juncheng Li, Guangwei Gao, Zhi Li, and Tiejong Zeng. 2023. Pft-ssr: Parallax fusion transformer for stereo image super-resolution. In *ICASSP*.
- [11] Lanqing Guo, Chong Wang, Wenhan Yang, Siyu Huang, Yufei Wang, Hanspeter Pfister, and Bihan Wen. 2023. Shadowdiffusion: When degradation prior meets diffusion model for shadow removal. In *CVPR*.
- [12] Zhi-min Guo et al. 2011. Research of hand positioning and gesture recognition based on binocular vision. In *IEEE International Symposium on VR Innovation*.
- [13] Jonathan Ho, Ajay Jain, and Pieter Abbeel. 2020. Denoising diffusion probabilistic models. *NeurIPS* (2020).
- [14] Jonathan Ho, Chitwan Saharia, William Chan, David J Fleet, Mohammad Norouzi, and Tim Salimans. 2022. Cascaded diffusion models for high fidelity image generation. *JMLR* (2022).
- [15] Yiwen Hua, Puneet Kohli, Pritish Uplavikar, Anand Ravi, Saravana Gunaseelan, Jason Orozco, and Edward Li. 2020. Holopix50k: A large-scale in-the-wild stereo image dataset. *arXiv preprint arXiv:2003.11172* (2020).
- [16] Jie Huang, Xueyang Fu, Zeyu Xiao, Feng Zhao, and Zhiwei Xiong. 2022. Low-light stereo image enhancement. *IEEE TMM* (2022).
- [17] Rongjie Huang, Jiawei Huang, Dongchao Yang, Yi Ren, Luping Liu, Mingze Li, Zhenhui Ye, Jinglin Liu, Xiang Yin, and Zhou Zhao. 2023. Make-an-audio: Text-to-audio generation with prompt-enhanced diffusion models. In *ICML*.
- [18] Daniel S Jeon, Seung-Hwan Baek, Inchang Choi, and Min H Kim. 2018. Enhancing the spatial resolution of stereo images using a parallax prior. In *CVPR*.
- [19] Bingxi Jia, Jian Chen, and Kaixiang Zhang. 2016. Drivable road reconstruction for intelligent vehicles based on two-view geometry. *IEEE Transactions on Industrial Electronics* (2016).
- [20] Diederik P Kingma and Max Welling. 2013. Auto-encoding variational bayes. *arXiv preprint arXiv:1312.6114* (2013).
- [21] Haoying Li, Yifan Yang, Meng Chang, Shiqi Chen, Huajun Feng, Zhihai Xu, Qi Li, and Yueting Chen. 2022. Srdiff: Single image super-resolution with diffusion probabilistic models. *Neurocomputing* (2022).
- [22] Jingyun Liang, Jiezhong Cao, Guolei Sun, Kai Zhang, Luc Van Gool, and Radu Timofte. 2021. Swinir: Image restoration using swin transformer. In *CVPR*.
- [23] Bee Lim, Sanghyun Son, Heewon Kim, Seungjun Nah, and Kyoung Mu Lee. 2017. Enhanced deep residual networks for single image super-resolution. In *CVPR workshops*.
- [24] Jianxin Lin, Lianying Yin, and Yijun Wang. 2023. Steformer: Efficient stereo image super-resolution with transformer. *IEEE TMM* (2023).
- [25] Shitong Luo and Wei Hu. 2021. Diffusion probabilistic models for 3d point cloud generation. In *CVPR*.
- [26] Moritz Menze and Andreas Geiger. 2015. Object scene flow for autonomous vehicles. In *CVPR*.
- [27] Axi Niu, Kang Zhang, Trung X Pham, Jinqiu Sun, Yu Zhu, In So Kweon, and Yanning Zhang. 2023. CDPMSR: Conditional Diffusion Probabilistic Models for Single Image Super-Resolution. *arXiv preprint arXiv:2302.12831* (2023).
- [28] Taragay Oskiper, Mikhail Sizintsev, Vlad Branzoi, Supun Samarasekera, and Rakesh Kumar. 2015. Augmented reality binoculars. *IEEE transactions on visualization and computer graphics* (2015).
- [29] Aditya Ramesh, Prafulla Dhariwal, Alex Nichol, Casey Chu, and Mark Chen. 2022. Hierarchical text-conditional image generation with clip latents. *arXiv preprint arXiv:2204.06125* (2022).
- [30] Robin Rombach, Andreas Blattmann, Dominik Lorenz, Patrick Esser, and Bjorn Ommer. 2022. High-resolution image synthesis with latent diffusion models. In *CVPR*.
- [31] Chitwan Saharia, William Chan, Huiwen Chang, Chris Lee, Jonathan Ho, Tim Salimans, David Fleet, and Mohammad Norouzi. 2022. Palette: Image-to-image diffusion models. In *SIGGRAPH*.
- [32] Chitwan Saharia, William Chan, Saurabh Saxena, Lala Li, Jay Whang, Emily L Denton, Kamyar Ghasemipour, Raphael Gontijo Lopes, Burcu Karagol Ayan, Tim Salimans, et al. 2022. Photorealistic text-to-image diffusion models with deep language understanding. *NeurIPS* (2022).
- [33] Chitwan Saharia, Jonathan Ho, William Chan, Tim Salimans, David J Fleet, and Mohammad Norouzi. 2022. Image super-resolution via iterative refinement. *IEEE TPAMI* (2022).
- [34] Daniel Scharstein, Heiko Hirschmüller, York Kitajima, Greg Krathwohl, Nera Nesić, Xi Wang, and Porter Westling. 2014. High-resolution stereo datasets with subpixel-accurate ground truth. In *Pattern Recognition*.
- [35] Shuyao Shang, Zhengyang Shan, Guangxing Liu, and Jinglin Zhang. 2023. Resdiff: Combining cnn and diffusion model for image super-resolution. *arXiv preprint arXiv:2303.08714* (2023).
- [36] Uriel Singer, Adam Polyak, Thomas Hayes, Xi Yin, Jie An, Songyang Zhang, Qiyuan Hu, Harry Yang, Oron Ashual, Oran Gafni, et al. 2022. Make-a-video: Text-to-video generation without text-video data. *arXiv preprint arXiv:2209.14792* (2022).
- [37] Jascha Sohl-Dickstein, Eric Weiss, Niru Maheswaranathan, and Surya Ganguli. 2015. Deep unsupervised learning using nonequilibrium thermodynamics. In *ICML*.
- [38] Jiaming Song, Chenlin Meng, and Stefano Ermon. 2020. Denoising diffusion implicit models. *arXiv preprint arXiv:2010.02502* (2020).
- [39] Wonil Song, Sungil Choi, Somi Jeong, and Kwanghoon Sohn. 2020. Stereoscopic image super-resolution with stereo consistent feature. In *AAAI*.
- [40] Yang Song, Jascha Sohl-Dickstein, Diederik P Kingma, Abhishek Kumar, Stefano Ermon, and Ben Poole. 2020. Score-based generative modeling through stochastic differential equations. *arXiv preprint arXiv:2011.13456* (2020).
- [41] Hugo Touvron, Thibaut Lavril, Gautier Izacard, Xavier Martinet, Marie-Anne Lachaux, Timothée Lacroix, Baptiste Rozière, Naman Goyal, Eric Hambro, Faisal Azhar, et al. 2023. Llama: Open and efficient foundation language models. *arXiv preprint arXiv:2302.13971* (2023).
- [42] Aaron Van Den Oord, Oriol Vinyals, et al. 2017. Neural discrete representation learning. *NeurIPS* (2017).
- [43] Jianyi Wang, Zongsheng Yue, Shangchen Zhou, Kelvin CK Chan, and Chen Change Loy. 2023. Exploiting diffusion prior for real-world image super-resolution. *arXiv preprint arXiv:2305.07015* (2023).
- [44] Longguang Wang, Yulan Guo, Yingqian Wang, Zhengfa Liang, Zaiping Lin, Jungang Yang, and Wei An. 2020. Parallax attention for unsupervised stereo correspondence learning. *IEEE TPAMI* (2020).
- [45] Longguang Wang, Yingqian Wang, Zhengfa Liang, Zaiping Lin, Jungang Yang, Wei An, and Yulan Guo. 2019. Learning parallax attention for stereo image super-resolution. In *CVPR*.
- [46] Yingqian Wang, Longguang Wang, Jungang Yang, Wei An, and Yulan Guo. 2019. Flickr1024: A large-scale dataset for stereo image super-resolution. In *CVPR Workshops*.
- [47] Yingqian Wang, Xinyi Ying, Longguang Wang, Jungang Yang, Wei An, and Yulan Guo. 2021. Symmetric parallax attention for stereo image super-resolution. In *CVPR*.
- [48] Bin Xia, Yulun Zhang, Shiyin Wang, Yitong Wang, Xinglong Wu, Yapeng Tian, Wenming Yang, and Luc Van Gool. 2023. Diffir: Efficient diffusion model for image restoration. *arXiv preprint arXiv:2303.09472* (2023).
- [49] Qingyu Xu, Longguang Wang, Yingqian Wang, Weidong Sheng, and Xinpu Deng. 2021. Deep bilateral learning for stereo image super-resolution. *IEEE SPL* (2021).
- [50] Bo Yan, Chenxi Ma, Bahetiyaer Bare, Weimin Tan, and Steven CH Hoi. 2020. Disparity-aware domain adaptation in stereo image restoration. In *CVPR*.
- [51] Zizheng Yang, Mingde Yao, Jie Huang, Man Zhou, and Feng Zhao. 2022. Sir-former: Stereo image restoration using transformer. In *ACM MM*.
- [52] Xinyi Ying, Yingqian Wang, Longguang Wang, Weidong Sheng, Wei An, and Yulan Guo. 2020. A stereo attention module for stereo image super-resolution. *IEEE SPL* (2020).
- [53] Syed Waqas Zamir, Aditya Arora, Salman Khan, Munawar Hayat, Fahad Shahbaz Khan, and Ming-Hsuan Yang. 2022. Restormer: Efficient transformer for high-resolution image restoration. In *CVPR*.
- [54] Yulun Zhang, Kunpeng Li, Kai Li, Lichen Wang, Bineng Zhong, and Yun Fu. 2018. Image super-resolution using very deep residual channel attention networks. In *ECCV*.
- [55] Yulun Zhang, Yapeng Tian, Yu Kong, Bineng Zhong, and Yun Fu. 2018. Residual dense network for image super-resolution. In *CVPR*.